The Aeronautical Journal (2022), **126**, pp. 1265–1287
doi:10.1017/aer.2022.15

REGULAR PAPER
2022 ISABE Conference Paper

Aeroengine transient performance simulation integrated with generic heat soakage and tip clearance model

Z. Li, Y.-G. Li* and S. Sampath

School of Aerospace, Transport and Manufacturing, Cranfield University, Cranfield, Bedford MK43 0AL UK
*Corresponding author. Email: i.y.li@cranfield.ac.uk

Received: 6 January 2021; **Revised:** 8 November 2021; **Accepted:** 20 January 2022

Keywords: Heat soakage; Tip clearance; Transient performance; Thermodynamic performance simulation; Gas turbine engine

Abstract

The simulations and assessment of transient performance of gas turbine engines during the conceptual and preliminary design stage may be conducted ignoring heat soakage and tip clearance variations due to lack of detailed geometrical and structural information. As a result, problems with transient performance stability may not be revealed correctly, and corresponding design iterations would be necessary and costly when those problems are revealed at a detailed design stage. To make an engine design more cost and time effective, it has become important to require better transient performance simulations during the conceptual and preliminary design stage considering all key impact factors such as fuel control schedule, rotor dynamics, inter-component volume effect as well as heat soakage and tip clearance variation effects. In this research, a novel transient performance simulation approach with generically simplified heat soakage and tip clearance models for major gas path components of gas turbine engines including compressors, turbines and combustors has been developed to support more realistic transient performance simulations of gas turbine engines at conceptual and preliminary design stages. Such heat soakage and tip clearance models only require thermodynamic design parameters as input, which is normally available during such design stages. The models have been implemented into in-house transient performance simulation software and applied to a model twin-spool turbojet engine to test their effectiveness. Comparisons between transient performance simulated with and without the heat soakage and tip clearance effects demonstrate that the results are promising. Although the introduced heat soakage and tip clearance models may not be as accurate as that using detailed component geometrical information, it is able to include the major heat soakage and tip clearance effects and make the transient performance simulations and analysis more realistic during conceptual and preliminary engine design stage.

Nomenclature

A	heat transfer area (m^2)
AR	aspect ratio of blade
Coe	coefficient of effective wetted area
Cp	specific heat ($kJ/kg \cdot K$)
C	temperature gradient
CMF	continuity mass flow
CW	compressor work (W)
D	diameter (m)
dH	enthalpy drop of turbine per stage (J)
DH	enthalpy drop of turbine (J)
dp	dynamic pressure ($kg/(ms^2)$)
E	Young's modulus (Pa)
EFF	isentropic efficiency

This paper is a version of a presentation due to be given at the 2022 ISABE Conference

https://doi.org/10.1017/aer.2022.15 Published online by Cambridge University Press

EGT	exhaust gas temperature (K)
h	heat transfer coefficient
H	height or thickness (m)
I	moment of inertial (kg·m^2)
ICV	inter-component volume
IMF	imbalanced-mass flow
HPC	high pressure compressor
HPT	high pressure turbine
K	thermal diffusivity of the gas (m^2/s)
k	conductivity (W/m$^/$K)
L	length of component (m)
LPC	low pressure compressor
LPT	low pressure turbine
MA	mach number
M	mass (kg)
MF	mass flow (kg/s)
N	rotational speed (RPM)
n	number of stages or blades
P	total pressure (Pa)
PR	pressure ratio
Q	mass flow function
q	heat energy (J)
SL	stage loading
SR	space to chord ratio
T	total temperature (K)
TC	tip clearance (m)
TET	turbine entry temperature (K)
Th	thickness of metal (m)
TW	turbine power (W)
t	time (s)
Δt	time interval (s)
R	radius (m)
RG	universal gas constant (Jmol-1K-1)
U	total conductance (W/K)
UB	blade tip speed (m/s)
u	growth in length (m)
V	volume (m3)
Visc	viscosity of gas or air (kg/ms)
W	mass flow rate (kg/s)
XN1R	relative low spool corrected speed
XN2R	relative high spool corrected speed
α	expansion rate (m/K)
σ	Stefan-Boltzmann constant
ε	radiative emissivity
γ	specific Heat (J/kgK)
ρ	density (kg/m^3)
τ	thermal time constant
δ	thermal expansion or contraction (m)
υ	Poisson's ratio
Δ	mechanical expansion (m)
ϑ	total deflection of component (m)

Subscripts

ann	annulus
b	blade
B	burner or combustor

https://doi.org/10.1017/aer.2022.15 Published online by Cambridge University Press

c	casing
C	compressor
d	disc
D	diffusor
f	flow
h	hub
inner	inner side of tube
in	inlet
out	outlet
L	combustor liner
m	mean value
nom	original
outer	outer side of tube
P	primary zone of combustor
RB	reference parameter at combustor inlet
ref	referred component part or gas/air flow
stage	stage of compressor or turbine
scl	scaling factor
s	solid
T	turbine
t	tip
w	wetted
1	start of time interval
2	end of time interval

1.0 Introduction

As a result of increasing demand of engine performance, the design of high-performance gas turbine engines becomes more and more challenging and costly and takes a longer period of time to complete. If engine transient performance and handling stability can be assessed effectively using simulations at conceptual and preliminary design stages, it could help shorten design period and reduce costs.

Compared with steady state performance simulations, transient performance simulations are more complicated because of many more factors, such as inter-component volumes, rotor inertia, engine control, heat soakage and tip clearance variations.

The impact of inter-component volumes, rotor inertia and engine fuel control has been modelled successfully by applying volume dynamics, rotor dynamics and PID control, respectively [1]. However, the inclusion of heat soakage and tip clearance effects in engine transient performance simulations is more challenging as such effects are more engine dependent and heavily rely on detailed engine geometrical and structural information [2]. Such information is usually unavailable at conceptual and preliminary design stages.

Heat soakage is caused by the heat transfer between engine metals and air or gas flows. It may have a notable impact on engine transient performance during rapid transient manoeuvres. For example, it could lead a 20-30% longer time for engine to complete a transient process [1]. Bauerfeind was one of the early pioneers who researched heat soakage effects on turbofan engines and identified its importance for transient performance modelling [3]. Maccallum reported a 1.5–2.0% thrust reduction at the end of acceleration due to heat soakage for a typical single spool engine [4]. Maccallum investigated thermal effects on changes in compressor characteristics due to flow boundary layer and density changes [5]. In addition, Maccallum et al. found that surge is more likely to happen during a so-called hot re-slam process when an engine is rapidly re-accelerated following a deceleration from a fully soaked high power rating [6]. Tip clearance is affected by heat transfer and centrifugal stress. Pilidis & Maccallum carried out the modelling of thermal effects on tip clearance and demonstrated their impact on transient

https://doi.org/10.1017/aer.2022.15 Published online by Cambridge University Press

performance response [7]. Their research indicated that ignorance of heat soakage and tip clearance effects in transient performance simulations may result in significant prediction errors.

Relevant research has also been conducted in the past. For example, Elder [8] introduced a heat exchange method to update the delivery temperature of a compressor with the consideration of heat convection. Pilidis [9] presented a thermomechanical model of a compressor to calculate both primary gas heat transfer and the impact on tip clearance. Fiola [10] demonstrated a 1D finite difference approach to calculate heat transfer and tip clearance in a HP turbine. Naylor [2] developed a 2D finite volume method for heat transfer calculation of the HP compressor of the Trent 500, including convection and conduction and a ring method for tip clearance variation. Visser et al. [11] developed a generic heat transfer model in GSP for both steady state and transient performance simulations, respectively where the heat transfer model for the recuperator is based on 1D method and the heat transfer calculation for compressor, turbine and combustor using a 0D approach. Vieweg et al. [12] made comparisons between a traditional 0D heat soakage model with in-house code GTlab and a turbofan transient performance data. Chapman et al. [13] developed a tip clearance model by using a finite difference method for a single-stage turbine. However, the methods mentioned above are either limited to the heat soakage effects on particular gas turbine components or rely on accurate geometrical information.

In this study, a new generically simplified method to simulate the heat soakage and tip clearance effects for three key gas path components — including compressors, combustors and turbines — has been introduced for the purpose of transient performance simulations with an objective that the method can be utilised during gas turbine engine conceptual and preliminary design stages when the accurate geometrical information of the engines are not available.

2.0 Methodology

2.1 Transient performance simulation method

Transient performance simulation is employed to assess gas turbine engine dynamic behaviour from one steady state to another. During transient process, the continuity of mass flow between engine components and the conservation of work on the same shaft are broken. The key impact factors on transient performance are rotor inertia, inter-component volumes and fuel control schedule.

To consider the effect of rotor inertia, rotor dynamics is applied where the unbalanced shaft power SP will drive the engine to either accelerate or decelerate based on rotor dynamics presented by Equation (1)

$$SP = TW - CW = \frac{dN}{dt} * I * N * \left(\frac{\pi}{30}\right)^2 \tag{1}$$

where TW is the turbine power and CW is the compressor power. The shaft rotational speed at the transient process can be determined by Euler's method shown by Equation (2)

$$N(t + \Delta t) = \frac{dN}{dt} * \Delta t + N(t) \tag{2}$$

The inter-component volume effect may be dealt with by two methods in gas turbine transient performance simulations, one called Continuous Mass Flow (CMF) method [14] and the other called Inter-Component Volume (ICV) method [15]. In this study, an improved CMF method called the Imbalanced Mass Flow (IMF) [16] method is used to capture the volume packing effect. The imbalanced mass flow term (IMF) is calculated by volume dynamics, and its effect is applied to the corresponding component for mass flow rebalancing during the iterative calculation process. Such calculation is given by Equations (3) and (4).

$$IMF = W_1 - W_2 \tag{3}$$

$$IMF = \frac{\mathrm{dm}}{dt} = \frac{dP}{dt} * \frac{V}{RT} \tag{4}$$

https://doi.org/10.1017/aer.2022.15 Published online by Cambridge University Press

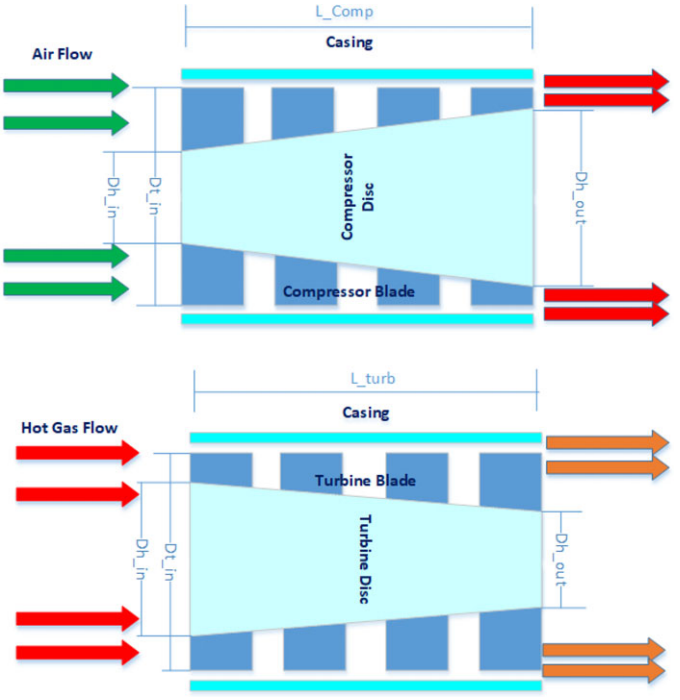

Figure 1. *Generic turbomachine geometry.*

where W_1 is in-coming flow rate and W_2 is out-going flow rate of an inter-component volume. Due to the limited space in the paper, no further details of the IMF method are presented, and the interested readers may refer to Ref. (16).

In addition, fuel control is also very important for transient performance simulations. In this paper, a simple fuel schedule where fuel flow varies with the corrected shaft speed of the engine is applied.

2.2 Geometry model

A geometry model is normally built on exact geometry of the key gas path components concerned, such as compressors, combustors and turbines of gas turbine engines. However, such information is not available at engine conceptual and preliminary design stages and therefore heat soakage and tip clearance variations have to be ignored in transient performance simulations in the past. In this study, a simplified geometry model is set up based on design point engine performance parameters and basic component design criteria to establish the necessary geometrical data of major gas path components required for transient performance simulations with the aim of capturing major heat soakage and tip clearance variation effects.

2.2.1 Axial compressors and turbines

Figure 1 represents the simplified geometry models for generic axial compressors and turbines. It is assumed that both of them consist of three parts: blades, casing and discs with constant external diameter D_t. It is also assumed that the basic aerothermal design criterion for compressors and turbines are given in Table 1 [17].

https://doi.org/10.1017/aer.2022.15 Published online by Cambridge University Press

Table 1. *Basic turbomachinery design criteria*

Component	Max Tip Speed Ut.max (m/s)	Inlet/Outlet Mach No.	Length of Single Stage (m)	Stage Pressure Ratio	Stage Loading
Compressors	400-450	0.3-0.45	0.07	1.365	/
Turbines	400-430	0.3-0.5	0.07	/	2.2

The outer annulus diameter D_t is estimated by Equation (5) using the shaft rational speed RPM at the design point:

$$D_t = \frac{UB_{t,max}}{RPM * \pi * 60} \tag{5}$$

The flow annulus cross area A_{ann} is calculated by Equation (6)

$$A_{ann} = \frac{W\sqrt{T}}{PQ} \tag{6}$$

where mass flow function Q is given by Equation (7)

$$Q = MA * \sqrt{\frac{\gamma}{R}} * \left(1 + \frac{\gamma - 1}{2} * M^2\right)^{\left(-\frac{\frac{\gamma+1}{2}}{\gamma-1}\right)} \tag{7}$$

The hub diameter D_{h} of the turbomachinery component can be estimated by Equation (8)

$$D_h = \sqrt{\frac{A_t - A_{ann}}{\pi}} * 2 \tag{8}$$

The number of stages $n_{C,\,stage}$ of a compressor is estimated by the ceiling function Equation (9) to estimate the least number of the stages required to achieve the required overall pressure ratio for compressors

$$n_{C,\,stage} = Ceiling\left[\log_{1.35} PR\right] \tag{9}$$

where PR is the compressor pressure ratio and the value of 1.35 is the average stage pressure ratio at design point representing the state-of-the-art compressor technology such as that of the GE9X with a total pressure ratio of 27 and stage number of 11. The number of stages $n_{T,\,stage}$ of a turbine is estimated by Equation (10) to achieve the required total enthalpy drop for the turbine through stage loading and blade tip speed.

$$n_{T,\,stge} = Ceiling\left[\frac{DH}{SL * UB_{t,max}{}^2}\right] \tag{10}$$

where DH is the total enthalpy drop; SL is the stage loading; $UB_{t,max}$ is blade tip speed. The length L of the turbomachinery component is estimated by Equation (11).

$$L = n_{sta} * L_{stage} \tag{11}$$

Due to the existence of the interface surface between disc and blade, the effective wetted area $A_{d,w}$ of a disc is estimated by Equation (12).

$$A_{d,w} = \pi * D_{h,m} * L * Coe \tag{12}$$

Consequently, the total interface A_{bd} between the blade and the disc is estimated by

$$A_{bd} = \pi * D_{h,m} * L * (1 - Coe) \tag{13}$$

Then the number of the blades in the intermediate stage can be estimated by Equation (14).

$$n_{b,stage} = 2 * \pi * \frac{D_t + D_{h,m}}{SR * D_t - D_{h,m}/AR} \tag{14}$$

https://doi.org/10.1017/aer.2022.15 Published online by Cambridge University Press

It is assumed that the number of blades is the same in each stage. Therefore, the total effective wetted area of the blades in the primary flow path is estimated by Equation (15).

$$A_{b,w} = n_b * n_{stage} * \frac{\left(D_t - D_{h,m}\right)^2}{AR} \tag{15}$$

The total volume of the blades V_b and the casing V_c can be represented by the corresponding surface area A multiplied by the thickness H by Equation (16).

$$V = A * H \tag{16}$$

The disc volume V_d is calculated by the mean cross-section area multiplied by the length as shown in Equation (17) where the space inside the disc is considered by coefficient 0.5.

$$V_d = \pi * \left(\frac{D_{h,m}}{2}\right)^2 * L * 0.5 \tag{17}$$

The metal mass of each component is estimated by Equation (18).

$$\mathrm{M} = V * \rho \tag{18}$$

As the shapes of the disc and blades are non-uniform in axial direction, the mass function per unit length M(x) of them are considered. For compressor disc, it is assumed that its inlet diameter is equal to half of its hub mean diameter and the outlet diameter is equal to one and a half of the hub mean diameter. Therefore, the linear relationship of the compressor disc diameter $D_d(x)$ could be expressed by Equation (19).

$$D_d(x) = \frac{D_{h,m}}{L}x + \frac{D_{h,m}}{2} \tag{19}$$

By substituting Equation (19) into Equations (17) and (18), the mass function of the compressor disc is given by Equation (20).

$$\mathrm{M}_d(x) = \pi * \left(\frac{D_{h,m}}{2L}x + \frac{D_{h,m}}{4}\right)^2 * 0.5 * \rho \tag{20}$$

For the compressor blades, the mass distribution in axial direction could be treated the same way as that of the discs. As the tip diameter is constant, the cross-section area of the blade rows could be presented by Equation (21).

$$A_b(x) = \pi * \left[\left(\frac{D_t}{2}\right)^2 - \left(\frac{D_{h,m}}{2L}x + \frac{D_{h,m}}{4}\right)^2\right] \tag{21}$$

Thus, the mass function of the compressor blades $M_b(x)$ can be represented by Equation (22).

$$\mathrm{M}_b(x) = \pi * \left[\left(\frac{D_t}{2}\right)^2 - \left(\frac{D_{h,m}}{2L}x + \frac{D_{h,m}}{4}\right)^2\right] * \rho \tag{22}$$

According to Equation (13), the interface area function $A_{bd}(x)$ between the blades and the disc is estimated by Equation (23).

$$A_{bd}(x) = \pi * \left(\frac{D_{h,m}}{}x + \frac{h,m}{2}\right) * (1 - Coe) \tag{23}$$

Similarly, it is also assumed that the inlet diameter of the turbine disc is equal to one and a half of its hub mean diameter and the outlet diameter of the turbine disc is equal to half of the hub mean diameter. Therefore, the linear variation of the turbine disc diameter $D_d(x)$ along axial direction could be expressed by Equation (24)

$$D_d(x) = -\frac{D_{h,m}}{L}x + \frac{3D_{h,m}}{2} \tag{24}$$

https://doi.org/10.1017/aer.2022.15 Published online by Cambridge University Press

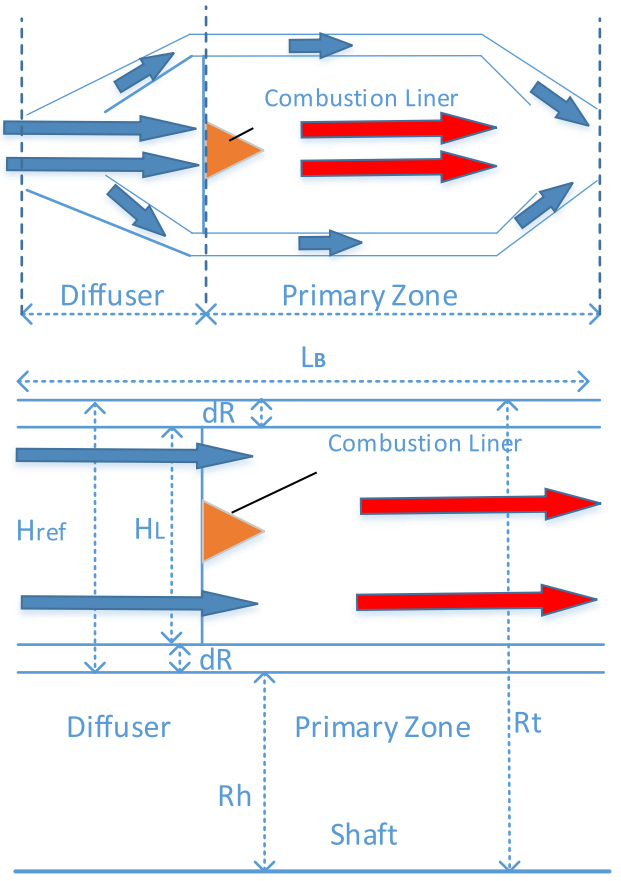

Figure 2. *Generically simplified combustor.*

Consequently, the mass function of the turbine disc and blades are represented by Equations (25) and (26), respectively.

$$\mathrm{M}_d(x) = \pi * \left(-\frac{D_{h,m}}{2L}x + \frac{3D_{h,m}}{4}\right)^2 * 0.5 * \rho \tag{25}$$

$$\mathrm{M}_b(x) = \pi * \left[\left(\frac{D_t}{2}\right)^2 - \left(-\frac{D_{h,m}}{2L}x + \frac{3D_{h,m}}{4}\right)^2\right] * \rho \tag{26}$$

As the casing of the compressor and turbine has a constant diameter and could be regarded as being uniform, the casing mass function in axial direction could be given by Equation (27).

$$\mathrm{M}_c(x) = \frac{\mathrm{M_c}}{L} \tag{27}$$

2.2.2 Combustor

The simplified combustor is assumed to be of annular type with double casing shown in Fig. 2. The whole combustor is divided into two parts: a diffuser and a primary zone.

The combustor reference area at combustor inlet A_{ref} is represented by Equation (28) [18] where the pressure drop factor $\frac{\Delta P_{3-4}}{q_{ref}}$ for annular combustor is assumed to be 20, and the corresponding pressure

https://doi.org/10.1017/aer.2022.15 Published online by Cambridge University Press

loss factor $\frac{\Delta P_{3-4}}{P_3}$ is assumed to be 0.06. RG is the universal gas constant.

$$A_{RB} = \left[\frac{RG}{2} \left(\frac{\dot{m}_3 T_3^{0.5}}{P_3} \right)^2 \frac{\Delta P_{3-4}}{dp} \left(\frac{\Delta P_{3-4}}{P_3} \right)^{-1} \right]^{0.5} \tag{28}$$

The distance dR between the inner casing and the outer casing is estimated by Equation (29)

$$dR = 0.2 * R_{h,out} \tag{29}$$

where $R_{h,out}$ is the upstream compressor rear stage hub diameter. The height of the combustor inlet is calculated by Equation (30).

$$H_{RB} = \sqrt{\frac{A_{RB} + \pi * {R_h}^2}{\pi}} - R_h \tag{30}$$

Hence, the height of the combustor liner H_L is estimated by Equation (31).

$$H_L = H_{RB} - 2 * dR \tag{31}$$

As the modern annular combustor is designed short axially, the length of the annular combustor L_B is roughly two times the height of its liner H_L. Hence, the total length of the combustor is given by Equation (32).

$$L_B = H_L * 2 \tag{32}$$

It is assumed that the length of the combustor diffuser L_D is half of that of the liner length so L_D is calculated by Equation (33).

$$L_B = H * 0.5 \tag{33}$$

It is assumed that it has double casing configuration, so the total wetted area of the combustor $A_{B,w}$ is the sum of the wetted area of the inner casing $A_{B,inner,w}$ and the outer casing $A_{B,outer,w}$ as shown by Equation (34) where the wetted areas could be estimated by the multiplication between corresponding perimeter and length.

$$A_{B,w} = A_{B,inner,w} + A_{B,outter,w} \tag{34}$$

It is also assumed that the combustor casing thickness H_B is uniform, and therefore the volume of the combustor casing metal V_B is calculated by the sum of the volumes of the inner casing $V_{B,inner}$ and the outer casing $V_{B,outer}$ shown by Equation (35).

$$V_B = V_{B,inner} + V_{B,outer} = (A_{B,inner,w} + A_{B,outter,w}) * H_B \tag{35}$$

Finally, the metal mass of each part of the combustor could be determined by Equation (18).

As the combustor could be regarded as a duct, its mass function could be expressed by Equation (27) as well. Similarly, the combustor area function could be presented by Equation (36)

$$A_{B,w}(x) = \frac{A_{B,inner,w} + A_{B,ou,w}}{L} \tag{36}$$

2.3 Heat transfer model

Assumptions for the heat transfer model are made as followings:

- Conductive heat transfer is only considered between air/gas and component metals in radial direction.
- No conductive heat transfer between the components.
- No heat loss to ambient environment.
- All temperature profiles within the components are the same in radial direction and vary linearly along the axial direction.

https://doi.org/10.1017/aer.2022.15 Published online by Cambridge University Press

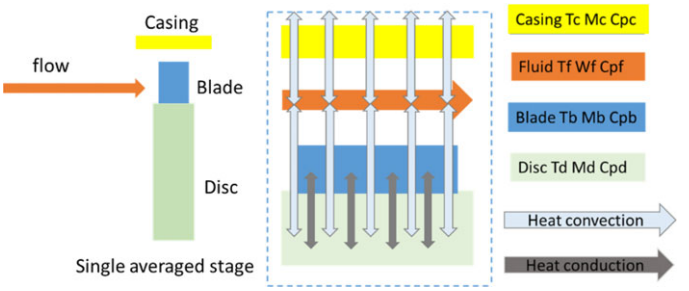

Figure 3. *Heat transfer model for turbomachinery.*

- The metal mass profile functions defined as the mass per unit axial length vary linearly along the axial direction.
- The wetted area profile functions of all components defined as the area per unit axial length are linear along the axial direction.
- The heat transfer coefficients are linear along the axial direction.
- No heat loss in air system or from cooling flows.

The heat transfer models developed in this study is to capture the thermal effects of the following:

1. Convective heat transfer between the gas flow in the main gas path and the turbomachinery and the combustor metals.
2. Radiative heat transfer between the gas flow and the combustor metals.
3. Conductive heat transfer between the blades and the discs in the turbomachinery components.

2.3.1 Turbomachinery heat transfer model

The left side of Fig. 3 shows a schematic of the turbomachinery components, including casing, blades and discs, and the right side of the figure shows a schematic of the heat transfer between them where convective and conductive heat transfers are considered.

2.3.1.1 Convective heat transfer. The convective heat transfer between air/gas flow and component metals is calculated based on the lumped capacitance method by Equation (37) with time constant.

$$\frac{dq}{dt} = \mathrm{M}_s * Cp * \left(T_f - T_s\right)\left(e^{-\frac{\Delta t}{\tau}} - 1\right) \tag{37}$$

$$\tau = \mathrm{M}_s * \frac{Cp}{h * A} \tag{38}$$

The heat transfer coefficients used in this paper refer to Ref. (2). For forced convection of flow through a duct,

$$h = 0.36 * \mathrm{Re}^{0.8} Pr^{\frac{1}{3}} \left(\frac{D}{L}\right)^{\frac{1}{18}} \left(\frac{Visc}{Viscw}\right)^{0.14} \frac{K}{D} \; if \; (\mathrm{Re} > 2,100) \tag{39}$$

$$h = 1.86 * \mathrm{Re}^{\frac{1}{3}} Pr^{\frac{1}{3}} \left(\frac{D}{L}\right)^{\frac{1}{3}} \left(\frac{Visc}{Viscw}\right)^{0.14} \frac{K}{D} \; if \; (\mathrm{Re} \leq 2,100) \tag{40}$$

https://doi.org/10.1017/aer.2022.15 Published online by Cambridge University Press

For a forced convection of flow through a rotating disc,

$$h = 0.0267 * \frac{\mathrm{Re}^{0.6} Pr^{0.8} K}{R} \; if \;\; (Re \leq 24,000) \tag{41}$$

$$h = 0.616 * \frac{\mathrm{Re}^{0.5} Pr^{\frac{1}{3}} K}{R} \; if \; (Re > 24,000) \tag{42}$$

where the Reynold number Re for a rotating disc and a duct, and Prandtl number Pr are estimated by Equations (43) to (45),

$$\mathrm{Re} = (\rho * \omega * R^2)/Visc \tag{43}$$

$$\mathrm{Re} = W * D/(*Visc) \tag{44}$$

$$Pr = Cp * Visc/K \tag{45}$$

where D is the hydraulic diameter of a tube, L the length of the duct, K the thermal diffusivity of the gas, V_{isc} the bulk viscosity of the gas, V_{iscw} the viscosity of the gas at the wall temperature, and R the radius of the disc.

The linear temperature profiles $T_{ref}(x)$ in axial direction for the gas flow, the blades, the casing and the discs, are represented by Equation (46).

$$T_{ref}(x) = \frac{T_{ref,\,out} - T_{ref,n}}{L} * x + T_{ref,in} \tag{46}$$

where the subscrip "ref" refers to each component concerned. The axial heat transfer coefficient profiles for component metals $h(x)$ is represented by Equation (47).

$$h(x) = h_{in} + \frac{h_{out} - h_{in}}{L} * x \tag{47}$$

Substituting Equation (46) into Equation (37) and applying integration yields the total convective heat transfer between the air/gas flow and each part of component metal represented by Equation (48).

$$\int_0^L q_{conv} dx = \int_0^L M_{ref}(x) * Cp * \left(\frac{T_{f,out} - T_{in}}{L} - \frac{T_{ref,out} - T_{in}}{L} \right) * \left(e^{-\frac{\Delta}{\tau}} - 1 \right) dx \tag{48}$$

Where $T_{f,out}$ represents the outlet temperature of the air/gas flow, $T_{ref,out}$ the outlet temperature of the blades, the casing or the discs, and M_{ref}(x) is the metal mass profile functions defined as the mass per unit axial length and the subscript "*ref*" refers to the blades ("*b*"), the casing ("*c*") or the discs ("*d*") that is assumed to be linear and can be determined based on the designs in Section 2.2.

2.3.1.2 Conductive heat transfer. Figure 4 represents the conductive heat transfer between the blades and the discs estimated by the lumped capacitance method shown by Equation (49)

$$\frac{dq}{dt} = U_{total} * \; (T_b - T_d) \left(e^{-\frac{\Delta t}{Tau}} - 1 \right) \tag{49}$$

$$U_{total} = \frac{1}{\frac{1}{\frac{k_b * A_{bd}}{X_b}} + \frac{1}{\frac{k_d * A_{bd}}{X_d}}} \tag{50}$$

$$Tau = \frac{\mathrm{M}_b * Cp_b + \mathrm{M}_d * Cp_d}{\frac{k_b * A_{bd}}{X_b} + \frac{k_d * A_{bd}}{X_d}} \tag{51}$$

where U_{total} is the total thermal conductance of the blades and the discs, k_b is the conductivity of the blades, k_d is the conductivity of the discs, X_b is the distance between the centre of the blades and the

https://doi.org/10.1017/aer.2022.15 Published online by Cambridge University Press

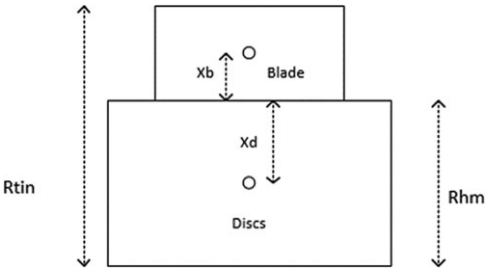

Figure 4. *Conductive heat transfer between blades and discs.*

interface, X_d is the distance between the centre of the discs and the interface, A_{bd} is the interface area between the blades and the discs, and T_{au} is the time constant of the conductive heat transfer.

Substituting the temperature profiles of the blades $T_b(x)$ and the discs $T_d(x)$ and the area profile function of the interface $A_{bd}(x)$ into Equation (49) derives the total conductive heat transfer calculated by Equation (52).

$$\int_0^L q_{cnd}dx = \int_0^L A_{bd}(x) * \left(\frac{T_{b,out} - T_{in}}{L} - \frac{T_{d,out} - T_{in}}{L}\right) * \frac{k_b k_d}{k_b X_d + k_d X_b} * \left(e^{-\frac{\Delta t}{Tau}} - 1\right) dx \tag{52}$$

where A_{bd}(x) is the area profile functions defined as the area per unit axial length that is assumed to be linear and can be determined based on the designs in Section 2.2.

For the turbomachinery system, the heat transfer happens among four subsystems, which are the air/gas flow, the blades, the casing and the discs. Based on energy conservation, the temperature variation of the air/gas flow over time is determined by the sum of the convection between the air/gas flow and the blades, the casing and the disc, represented by Equation (53).

$$\sum \int_0^L (q_{Conv,b} + q_{Conv,c} + q_{Conv,d})dx = \int_0^L W_f * \Delta t * Cp_f * \left[C_f(t + \Delta t) - C_f(t)\right] xdx \tag{53}$$

The temperature variation of the blades over time is determined by the sum of the convective heat $q_{conv,b}$ between the air/gas flow and the blade metal and the conductive heat q_{cond} between the blade and the disc metals represented by Equation (54).

$$\sum \int_0^L (q_{conv,b} + q_{cond})dx = \int_0^L \mathrm{M}_b(x) * Cp * [C_b(t + \Delta t) - C_b(t)]\, xdx \tag{54}$$

In a similar way, the temperature variation of the discs over time is determined by the sum of the convective heat $q_{conv,d}$ between the air/gas flow and the disc metal and the conductive heat q_{cond} between the blade and the disc metals represented by Equation (55).

$$\sum \int_0^L (q_{conv,d} + q_{cond})dx = \int_0^L \mathrm{M}_d(x) * Cp * [C_d(t + \Delta t) - C_d(t)]\, xdx \tag{55}$$

Finally, the temperature variation of the casing over time is determined by the convective heat $q_{conv,d}$ between the air/gas flow and the casing metal shown by Equation (56).

$$\sum \int_0^L q_{Conv,c}dx = \int_0^L \mathrm{M}_c(x) * Cp * [C_c(t + \Delta t) - C_c(t)]\, xdx \tag{56}$$

Hence, by solving the above four Equations (52) to (56), the four temperature gradients C_{ref} where the subscrip *ref* refers to the air/gas flow, the blades, the casings and the discs, respectively, can be obtained. Correspondingly, the exit temperatures of the air/gas flow, the blades, the casings and the discs can be updated by Equation (57).

https://doi.org/10.1017/aer.2022.15 Published online by Cambridge University Press

$$T_{ref,\,out}(t+\Delta t) = C_{ref}(t+\Delta t) * L + T_{ref,in}(t+\Delta t) \tag{57}$$

$$C_{ref} = \frac{T_{ref,\,out} - T_{ref,in}}{L} \tag{58}$$

where C_{ref} is temperature gradient where the subscript "*ref*" refers to the air/gas flow ("*f*"), the blades ("*b*"), the discs ("*d*") and the casing ("*c*").

2.3.2 Combustor heat transfer

Due to high gas temperature inside the combustor, the radiative heat transfer cannot be ignored. Therefore, the heat transfer model for combustors mainly considers convection and radiation. Consequently, it is reasonable to split the combustor into two sections, i.e. diffusion and primary zones due to significant temperature difference between the two parts.

It is assumed that the metal components in the combustor do not have conductive heat transfer between each other. The heat transfer in both the diffusor and the primary zone is mainly convection and radiation. The convective heat transfers for the diffusor $q_{conv,D}$ and the primary zone $q_{conv,P}$ could be calculated using Equation (48) where the subscript "ref" refers to either the diffusor or the primary zone.

The radiative heat transfer between the combustor metal and the gas flow at any axial position within the combustor is estimated by Equation (59)

$$q_{rad} = \sigma * \left(\frac{1+\varepsilon_w}{2}\right) * A_B * \left(\varepsilon_g T_f^4 - \alpha_g T_B^4\right)\left(e^{-\frac{\Delta t}{\tau}} - 1\right) \tag{59}$$

where ε_w and ε_g are radiative emissivity of the wall and the gas, respectively. α_g is gas absorptivity and σ the Stefan-Boltzmann constant. The total radiative heat transfer q_{rad} for both the diffusor $q_{rad,}$ and the primary zone $q_{rad,P}$ can be calculated by Equation (60).

$$\int_0^{L_{ref}} q_{rad,ref}\,dx = \int_0^{L_{ref}} ref(x) * \sigma * \left(\frac{1+\varepsilon_w}{2}\right)\left[\varepsilon_g\left(T_{f,in} + \frac{T_{f,out-}T_{f,in}}{L_{ref}}x\right)_{ref}^4 - \alpha_g\left(T_{B,in} + \frac{T_{B,out-}T_{B,in}}{L_{ref}}x\right)_{ref}^4\right]\left(e^{-\frac{\Delta t}{\tau_B}} - 1\right)dx \tag{60}$$

where $T_{f,in}$ and $T_{f,out}$ are the inlet and outlet gas temperature in the diffuser or the primary zone, respectively, $T_{B,in}$ and $T_{B,out}$ are the inlet and outlet metal temperature of the diffuser or the primary zone, respectively, and $A_{ref}(x)$ is the surface area profile function defined as the area per unit axial length. $A_{ref}(x)$ is assumed to be linear and can be determined based on the designs in Section 2.2.

According to the heat transfer model of the combustor system, the heat transfer process could be divided into three sub-systems, which are the heat transfer to or from the air/gas flow, the heat transfer to or from the diffuser metal and the heat transfer to or from the primary zone metal, respectively. Based on the conservation of energy, the total heat energy transferred to or from the air/gas flow is equal to the accumulative convective heat energy and the radiative heat energy between the air/gas and the combustor metals, as shown by Equation (61).

$$\sum \int_0^{L_B} (q_{conv} + q_{rad})dx = \int_0^{L_B} W_f * \Delta t * Cp_f * \left[C_f(t+\Delta t) - C_f(t)\right]dx \tag{61}$$

The total energy transferred to or from the diffuser metal is equal to the sum of convective energy $q_{conv,D}$ and radiative energy$q_{rad,D}$, as shown by Equation (62).

$$\sum \int_0^{L_D} (q_{conv,D} + q_{rad,D})\,dx = \int_0^{ref} \mathrm{M}_D(x) * Cp_B * \{C_D(t+\Delta t) - C_D(t)\}dx \tag{62}$$

https://doi.org/10.1017/aer.2022.15 Published online by Cambridge University Press

Similarly, total energy transferred to or from the primary zone metal is equal to the sum of the convective energy $q_{conv,P}$ and radiative energy $q_{rad,P}$, as shown by Equation (63).

$$\sum \int_0^{L_P} (q_{conv,P} + q_{rad,P})\, dx = \int_0^{L_P} M_P * Cp_B * \{C_P(t + \Delta t) - C_P(t)\} dx \tag{63}$$

where L_D and L_P stand for the length of the diffuser and the primary zone, respectively, and M_D (x) and M_P (x) represent the metal mass of the diffuser and the primary zone respectively. By solving Equations (61) to (63), the temperature gradients for the gas flow C_f, the diffusor metal C_D and the primary zone metal C_P can be obtained.

Once the temperature gradients for the three sub-systems become available, Equation (57) is applied to update the outlet temperature of the gas flow $T_{f,out}$, the diffuser metal $T_{D,out}$ and the primary zone metal $T_{P,out}$ by substituting the corresponding values of the combustor.

2.4 Tip clearance model

Compressor and turbine tip clearances could vary due to centrifugal force and thermal expansion or contraction of casing, blades and discs during engine transient processes. Consequently, the changing tip clearances could change the characteristics of the turbomachinery components.

The tip clearance model is divided into two parts: the tip clearance variation estimation and map correction. It is assumed that the tip clearance variation across a turbomachinery component is uniform and that only the expansion or contraction of blades, casing and discs in radial direction is considered.

2.4.1 Tip clearance variation

The thermal expansion or contraction Δ of blades, casing and discs due to changing temperature of the components can be estimated by Equation (64) [13]

$$\delta(t + \Delta t) = \alpha * H * [T(t + \Delta t) - T(t)] \tag{64}$$

where α is expansion rate and H the radius of the corresponding components.

The radial expansion or contraction of discs Δ_d and blades Δ_b due to centrifugal force are given by Equations (65) and (66) [19].

$$\Delta_d(t + \Delta t) = \frac{1}{4 * E_d} * (1 - \upsilon_d) * \rho_d * R_d^3 * \left(2 * P * \frac{N(t + \Delta t) - N(t)}{60}\right)^2 \tag{65}$$

$$\Delta_b(t + \Delta t) = \rho_b * H_b^2 * R_b / E_b * \left(2 * PI * \frac{N(t + \Delta t) - N(t)}{60}\right)^2 \tag{66}$$

The overall growth ϑ of the blades, casing and discs could be estimated by the summation of their thermal and mechanical growth by Equation (67)

$$\vartheta = \delta_c - (\delta_b + \Delta_b) - (\delta_d + \Delta_d) \tag{67}$$

Finally, the changing tip clearance *TC* is determined based on the tip clearance TC (t) at time t and its variation ϑ,

$$TC(t + \Delta t) = TC(t) + \vartheta \tag{68}$$

2.4.2 Map correction

According to Ref. (7), the characteristic map of a compressor could change due to the impact of heat transfer and tip clearance variation. Such map change could be represented by a shift of the speed lines

https://doi.org/10.1017/aer.2022.15 Published online by Cambridge University Press

Table 2. *Shaft speed correction coefficients [5]*

Compressor Type	Cl	C2	C3
Low Pressure	−0.07	0.07	0.3
High Pressure	−0.1	−0.1	0.3

of the map estimated by Equation (69)

$$\frac{\Delta N}{N} = C1 * \frac{\left(T_b - T_f\right)}{T_f} + C2 * \frac{\dot{Q}}{W_a * C_P * T_f} + C3 * \frac{\vartheta}{TC} \tag{69}$$

where the first term on the right side of the equation represents the effect of flow boundary layer development, the second term represents the effect of heat soakage, and the last term represents the tip clearance variation effect, and C1, C2 and C3 are corresponding coefficients that are compressor specific. These coefficients obtained from tests for low- and high-pressure compressors of a particular engine [5] are shown in Table 2 and used in this study.

Based on the estimated shift of the compressor shaft speed, the compressor map is corrected by scaling the map using the scaling factors calculated by Equations (70) to (72) referring to Ref. [20].

$$MF_{Scl} = \frac{MF\ (N + \Delta N)}{MF\ (N)} \tag{70}$$

$$PR_{Scl} = \frac{PR\ (N + \Delta N) - 1}{PR\ (N) - 1} \tag{71}$$

$$EFF_{Sc} = \frac{EFF\ (N + \Delta N\ )}{EFF\ (N)} \tag{72}$$

The explanation of the equations and their applications are as follows:

- A new shaft speed is obtained by estimating the change in shaft speed using Equation (69).
- Two sets of mass flow, pressure ratio and efficiency are obtained using the original map at shaft speed N and $(N + \Delta N)$, respectively.
- The scaling factors of mass flow, pressure ratio and efficiency are calculated by Equations (70) to (72) at the transient operating point represented by the shaft speed at N.
- The map is corrected by applying the scaling factors.
- Finally, the engine transient performance is updated using the corrected map.

The same map correction approach is also applied to turbines and therefore no further details are repeated.

2.5 Integration of models

The transient performance simulation system considering heat soakage and the impact of tip clearance variation has been established and illustrated in Fig. 5. This architecture of the whole system clearly shows the relationship and communication between the performance model and the heat soakage and tip clearance models.

3.0 Application and analysis

3.1 Engine model

The heat soakage and tip clearance models have been integrated with TurboCycle software and applied to a model twin-spool turbojet engine shown in Fig. 6. Table 3 gives the key performance specification

https://doi.org/10.1017/aer.2022.15 Published online by Cambridge University Press

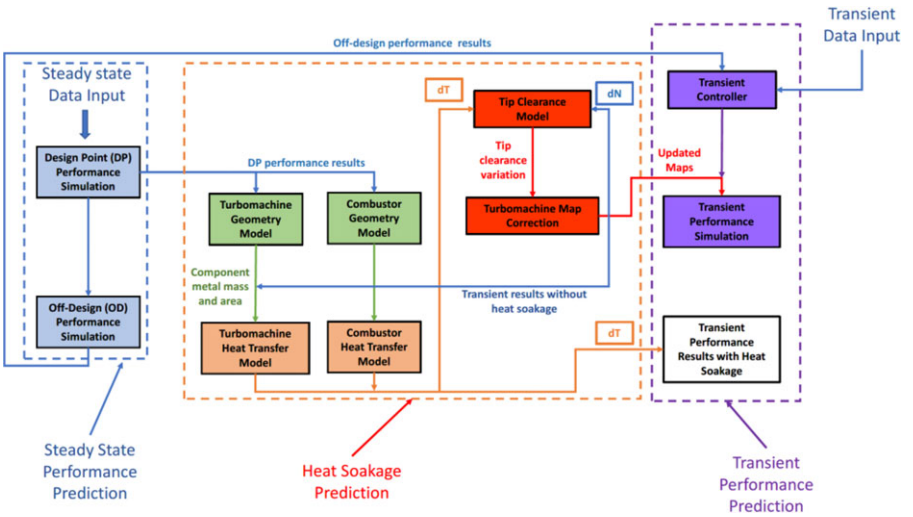

Figure 5. *Transient performance simulation system with impact of heat soakage and tip clearance variation.*

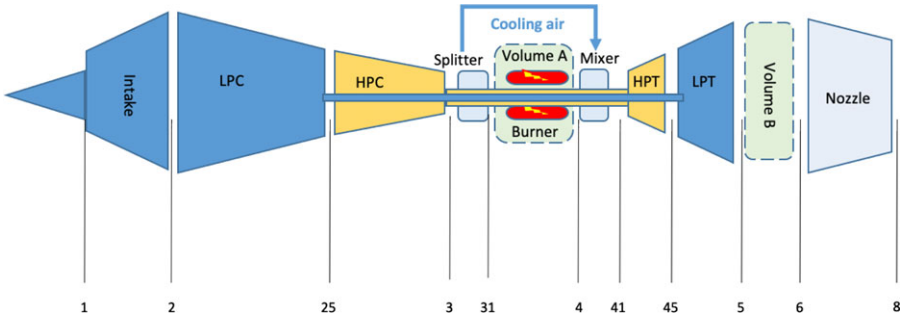

Figure 6. *Schematic of model twin-spool turbojet.*

of the model engine at sea level static ISA condition. The LP shaft corrected relative speed is set as the engine control parameter, or handle parameter to control the engine operating conditions.

3.2 Engine model verification

To verify the baseline engine model set up in TurboCycle the same engine model has been created in commercial software GasTurb [21] with the same model configuration, component maps, performance specification and fuel control schedule but without the inclusion of heat soakage and tip clearance models. Then the steady state and the transient performance of both engine models have been calculated and the results are compared with each other.

Regarding the verification of the steady state performance for the model, the part-load performance of the engine model indicated by different LP shaft rotational speed is simulated by both software packages and a comparison of the simulation results of selected performance parameters including net thrust (FN), fuel flow rate (WFE), turbine entry temperature (T41) and exhaust gas temperature (T5) are shown in Fig. 7. It can be seen that the TurboCycle model produces very close part-load performance to that of the GasTurb model.

https://doi.org/10.1017/aer.2022.15 Published online by Cambridge University Press

Table 3. *Engine performance specification at sea level static ISA condition*

Parameters	Value
Air mass flow (kg/s)	77.2
LPC pressure ratio	4.0
HPC pressure ratio	5.0
LPC isentropic efficiency	0.86
HPC isentropic efficiency	0.84
Burner efficiency	0.99
Turbine entry temperature (K)	1,150
HPT isentropic efficiency	0.89
LPT isentropic efficiency	0.9
LP speed (RPM)	9,000
HP speed (RPM)	14,000
Volume A (m^3)	0.2
Volume B (m^3)	0.2
Net thrust (kN)	44.3
SFC (g/kN/s)	18.36

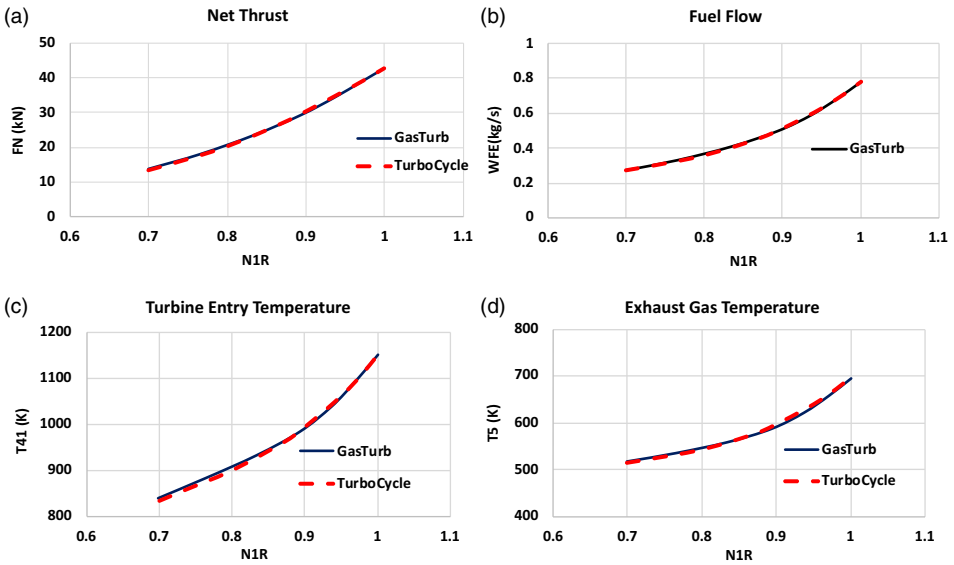

Figure 7. *Comparison of steady state performance between TurboCycle and GasTurb models (a)–(d).*

The verification of the engine model on simulated transient performance is conducted with an acceleration process from idle (70%) to full power (100%) using the same fuel control schedule as shown in Fig. 8.

Figure 9 shows a comparison of the simulation results of selected performance parameters including the corrected relative LP shaft speed (XN1R), air mass flow rate (W2), turbine entry temperature (T41) and net thrust (FN) of both models during the transient process. It can be seen that the simulated transient performance results of the TurboCycle model are also very close to those of the GasTurb model. Therefore, it has proven that the TurboCycle model is accurate enough as a baseline model to investigate the heat soakage and tip clearance variation effects in this study.

https://doi.org/10.1017/aer.2022.15 Published online by Cambridge University Press

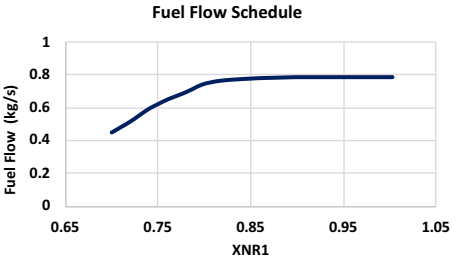

Figure 8. *Fuel schedule during acceleration.*

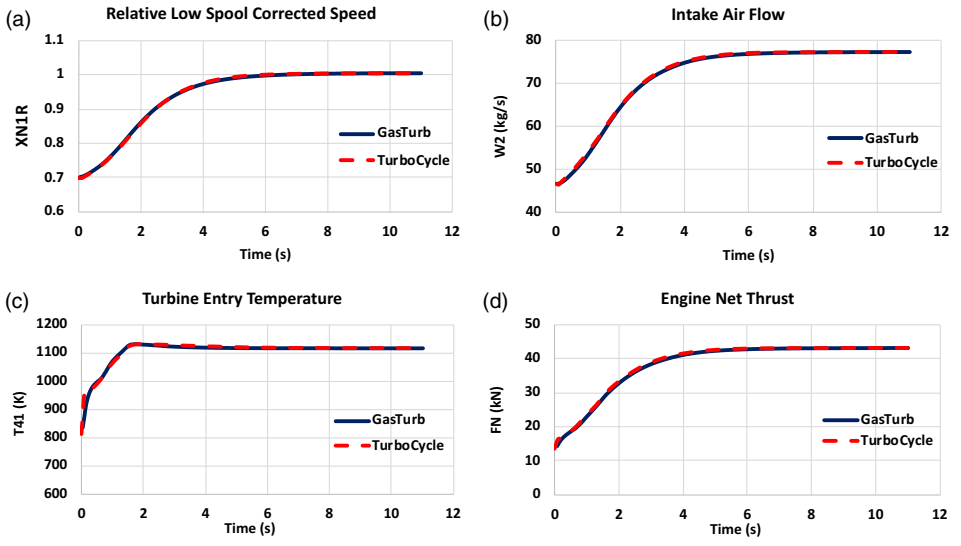

Figure 9. *Comparison of transient performance between TurboCycle and GasTurb models (a)–(d).*

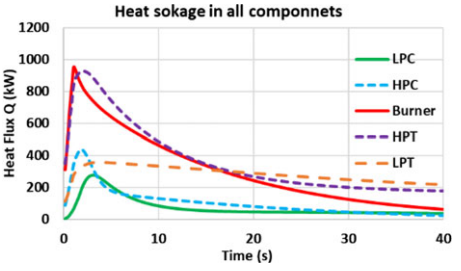

Figure 10. *Heat flux of individual components during acceleration.*

3.3 Transient performance affected by heat soakage and tip clearance variation

The heat soakage and tip clearance variation effects have been simulated by TurboCycle with the model twin-spool turbojet engine for the same acceleration process, i.e. from idle (70%) to full power (100%) using the same fuel schedule. The transient performance without the consideration of heat soakage and tip clearance variation is regarded as the baseline condition. To investigate and compare the heat soakage effect contributed by different components, the heat flux of individual components during the acceleration process are presented in Fig. 10.

https://doi.org/10.1017/aer.2022.15 Published online by Cambridge University Press

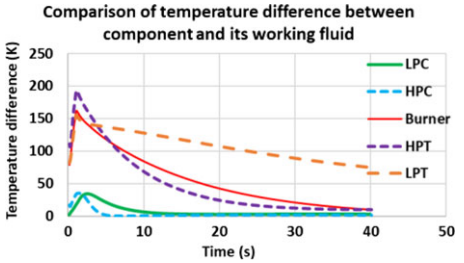

Figure 11. *Temperature difference between metal and gas flow of individual components during acceleration.*

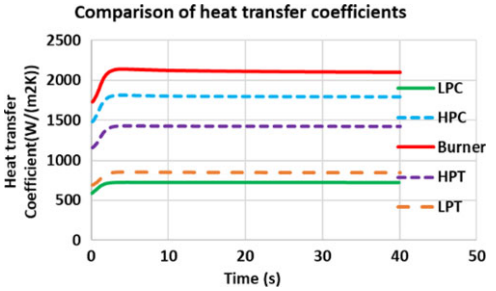

Figure 12. *Heat transfer coefficient of individual components during acceleration.*

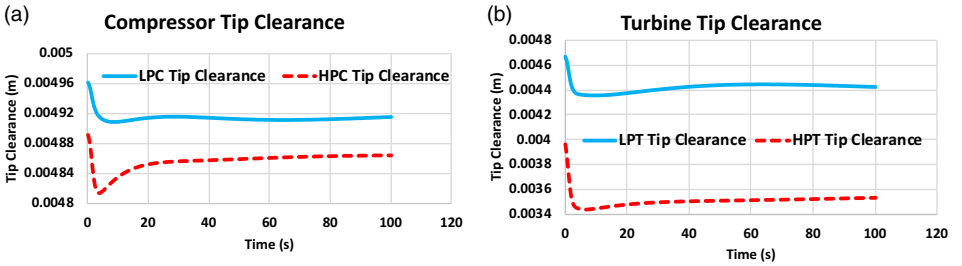

Figure 13. *Tip clearance variations in compressors and turbines (a)–(b).*

It can be seen that at the beginning of the acceleration, the heat transfer in the combustor is the greatest due to the excessive fuelling, which can produce extremely high level of radiative and convective heat flux. The heat flux of HPT becomes dominant after three seconds because of the highest increasing temperature of gas flow passing the HPT and the third highest heat transfer coefficient shown in Figs 11 and 12. The heat flux of LPT is weaker than that of the burner and HPT but stronger than that of LPC and HPC because of the higher temperature in LPT. LPC has the lowest heat flux due to its lowest temperature and the lowest heat transfer coefficient as illustrated in Figs 11 and 12.

The simulation results of the transient performance with the inclusion of the tip clearance variations of the turbomachinery components are presented in Fig. 13. It can be observed that at the beginning of the transient process, the tip clearance drops significantly because of the quick expansion of the blades due to centrifugal force. Then the tip clearance increases because of the gradual expansion of the casing heated by high temperature gas flow. In addition, the tip clearance variations of the high-pressure spool components are slightly more obvious than those of the low spool components because of the shaft rotational speed difference.

https://doi.org/10.1017/aer.2022.15 Published online by Cambridge University Press

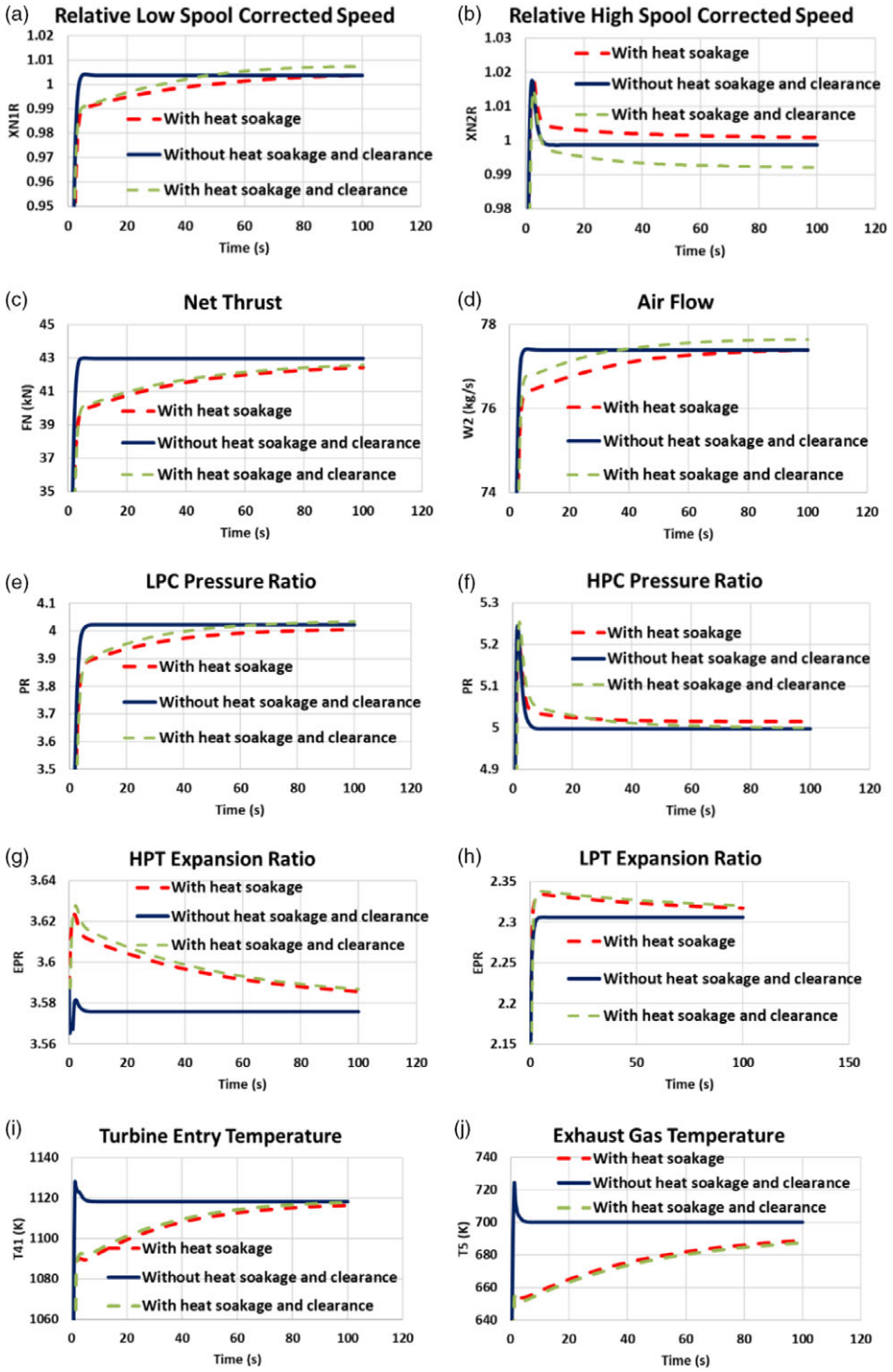

Figure 14. *Comparisons between transient performance with and without heat soakage and tip clearance variation effects (a)–(j).*

https://doi.org/10.1017/aer.2022.15 Published online by Cambridge University Press

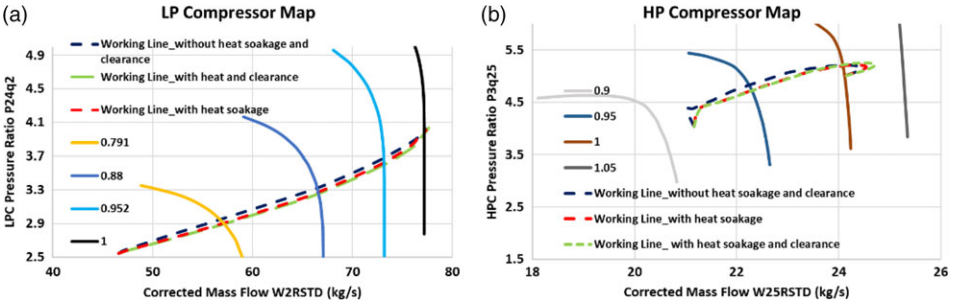

Figure 15. *Trajectories on compressor maps affected by heat soakage and tip clearance variation (a)–(b).*

To assess the impact of the heat soakage and tip clearance variation effects, the transient performance of the engine model in acceleration process with and without the heat soakage and tip clearance variation has been simulated using the same fuel schedule (Fig. 8). Figure 15 presents a comparison of the variations of selected performance parameters during the acceleration, including corrected relative LP and HP shaft speeds, net thrust, air flow rate, and pressure ratios of LPC, HPC, HPT and LPT, TET and EGT. It can be seen that the heat soakage and tip clearance variations would have significant impact on the acceleration time, and therefore would delay the response of the net thrust and other performance parameters.

In more details, compared with the baseline condition where no heat soakage and tip clearance variation are considered, the heat soakage alone causes the following effects for the acceleration process:

- Delay the corrected relative low pressure shaft speed reaching the target value from 10s to 100s, Fig. 14(a). It therefore causes a delay of the increase of the air flow rate (Fig. 14(d)) and the LPC pressure ratio (Fig. 14(e)).
- The corrected relative high pressure shaft speed becomes slightly higher due to the lower inlet temperature to the HPC caused by the heat soakage of LPC, Fig. 14(b). Consequently, the pressure ratio of the HPC also becomes slightly higher as shown in Fig. 14(f).
- The increase of the net thrust (Fig. 14(c)) is delayed even at the end of the 100-second acceleration process, which is about 1.27% lower than that without heat soakage.
- The increase of TET (Fig. 14(i)) has been significantly delayed by about 100s. Consequently, the corresponding expansion ratios of both HPT and LPT (Fig. 14(g) and (h)) become higher due to the increase of the corrected relative shaft speeds of HPT and LPT, as shown in Fig. 14(g)–(h).
- The increase of EGT has also been delayed tremendously. As a result, the net thrust is reduced due to the lower exhaust velocity caused by the delayed EGT, as shown in Fig. 14(j).

Further inclusion of tip clearance variation effect above the heat soakage effect would result in the following changes:

- Delay the LP corrected relative shaft speed (Fig. 14(a)) reaching the target value from 10s to 48s. In addition, the final LP corrected relative shaft speed is slightly higher than the baseline value.
- The corrected relative high pressure shaft speed (Fig. 14(b) becomes lower than the baseline value because the higher low pressure shaft speed would result in the higher LPC exit temperature.
- The variation of tip clearance has little impact on the net thrust as shown in Fig. 14(c).
- The increase of the air flow rate and the LPC pressure ratio is higher than that with heat soakage due to further rise of the low-pressure shaft speed, Fig. 14(d)–(e).

https://doi.org/10.1017/aer.2022.15 Published online by Cambridge University Press

Table 4. *Summary of impact of heat soakage and tip clearance variation at the end of 100 second of acceleration*

Parameters	Without Heat Soakage	With Heat Soakage	With Heat Soakage & Tip Clearance	Difference between with and without Heat Soakage	Difference between with Heat Soakage and with Heat Soakage & Tip Clearance [%]
Airflow (kg/s)	77.3932	77.3863	77.642	−0.0089	0.3304
LPC PR	4.0229	4.0052	4.0332	−0.4404	0.6997
HPC PR	4.9972	5.0149	4.999	0.3547	−0.3168
COT (K)	1156.3	1154.4	1155.7	−0.1686	0.1166
TET (K)	1118.2	1116.3	1117.8	−0.1699	0.1333
HPT PR	3.5758	3.5857	3.5867	0.2783	0.0278
LPT PR	2.3061	2.3174	2.3203	0.4890	0.1266
EGT (K)	700.1	688.8	687.5	−1.6095	−0.1882
FN (kN)	42.97	42.42	42.57	−1.2713	0.3436
XNlR	1.0038	1.0036	1.0073	−0.0199	0.3687
XN2R	0.9986	1.0009	0.9932	0.2303	−0.7693

- The pressure ratio of the HPC (Fig. 14(f)) becomes slightly lower than that with heat soakage and approaches the baseline value at the end of the acceleration.
- TET has a slight increase and approach its baseline value at the end of the acceleration, Fig. 14(i).
- The expansion ratios of HPT and LPT (Fig. 14(g) and (h)) have a slight increase compared to those with heat soakage only due to the slight increase of TET.
- EGT has a slight decrease and approaches its baseline value at the end of this acceleration, Fig. 14(j).

The acceleration trajectories of the LPC and the HPC at the baseline condition, with the heat soakage along, and with both the heat soakage and the tip clearance variation are shown in Fig. 15. It is obvious for the LPC that the heat soakage would lower the engine acceleration working line while adding the tip clearance variation would raise the acceleration working line slightly. The working line of the HPC is lowered by the heat soakage and tip clearance variation while the impact of adding the tip clearance variation on the working line is small.

A comparison of the most important performance parameters of the engine model at the end of the 100-second acceleration where the corrected low pressure shaft rotational speed reaches 100% with the heat soakage and the tip clearance variation compared with the baseline condition is summarised in Table 4. It can be seen that due to the heat soakage effect, TET has around -0.17% delay, EGT has about −1.61% delay, and the net thrust has about −1.3% delay. By adding extra tip clearance variation effect, TET increases by around 0.13%, EGT decreases by about 0.19%, and the net thrust increases by around 0.34%.

4.0 Conclusions

In this paper, a novel transient performance simulation approach with a simplified generic heat soakage and tip clearance model for key gas path components of a gas turbine engine, namely compressors, combustor and turbines, has been introduced. It may be less accurate compared with those using accurate geometrical and structural information of gas turbine engines but offers a reasonable solution to assess

https://doi.org/10.1017/aer.2022.15 Published online by Cambridge University Press

the engine transient performance and handling stability with the inclusion of heat soakage and tip clearance effects during their conceptual and preliminary design periods when detailed engine geometrical and structural information are not available. In-house software TurboCycle has been integrated with the heat soakage and tip clearance models to simulate the transient performance of gas turbine engines. The new method and software have been applied to a model twin-spool turbojet engine in an acceleration process with a time span of 100s of acceleration at sea level static ISA condition. With the heat soakage effect alone included, the time reaching the target value for the corrected low-pressure shaft rotational speed would be delayed by 90 seconds, while TET would be delayed by 100 seconds, and the net thrust would have about −1.3% shortfall at the end of the time span compared with those at the baseline condition. Meanwhile by adding the tip clearance variation effect, the corrected low-pressure shaft rotational speed reaching the target value would be delayed by 38 seconds, TET would be delayed by 80 seconds, and the net thrust would have 0.9% shortfall at the end of the time span compared with those at the baseline condition.

The results show that the introduced heat soakage and the tip clearance models are promising. In theory, this method can be applied to any other gas turbine engines and would help to assess the transient performance with heat soakage and tip clearance variation effects when engine geometrical and structural information is lacking.

References

[1] Thompson, B. Basic transient effects of aero-gas turbine, Ustaoset, Norway, 1974, AGARD CP151, paper number 2.
[2] Naylor, P. Gas turbine transient performance: Heat soakage modelling, PhD thesis, Cranfield University, 2004.
[3] Bauerfeind, K. Die exakte Bestimmung des Uebertragungsverhaltens von Turbostrahltriebwerken unter Berueckschtigung des instationaeren Verhaltens seiner Komponenten, PhD thesis in german, Fakultaet fuer Maschinenwesen und Elektrotechnik der Technischen Hochschule Muenchen, Germany, 1968.
[4] Maccallun, N.R.L. The performance of turbojet engines during the thermal soak transient, PhD thesis, Institute of Mechanical Engineers, 1970.
[5] Maccallun, N.R.L. Thermal influences in gas turbine transients-effects changes in compressor characteristics, The American Society of Mechanical Engineers, 79-GT-143, 1979.
[6] Maccallun, N.R.L. and Qi, O.F. The transient behavior of aircraft gas turbine, IMechE Seminar of Gas Turbines-Technology and Development, 1989.
[7] Pilidis, P. and Maccallum, N.R.L. The effects of heat transfer on gas turbine transients, The American Society of Mechanical Engineers, 86-GT-275, 1986.
[8] Elder, R. Effects of Heat Soakage in Axial Flow Compressors, American Society of Mechanical Engineers,
[9] Pilidis, P. Digital simulation of gas turbine performance, PhD thesis, University of Glasgow, 1983.
[10] Fiola, R. Berechnung des instationären Betriebsverhaltens von Gasturbinen unter besonderer Berücksichtigung von Sekundäreffekten, PhD thesis, TU München, 1993.
[11] Visser, W.P.J., et al. Modelling thermal effects on performance of small gas turbines, GT2015-42744, ASEM Turbo Expo 2015, 2015.
[12] Vieweg, M., et al. Comparison of a heat soakage model with turbofan transient engine data, GT2017-63461, ASME Turbo Expo 2017, 2017.
[13] Chapman, J., et al. *Integrated Turbine Tip Clearance and Gas Turbine Engine Simulation*, AIAA, 2016.
[14] Larrowe, V.L., Spencer, M.M. and Tribus, M. A Dynamic Performance Computer for Gas Turbine Engines Industry Program of the College of Engineering, Michigan University, 1957.
[15] Fawke, A.J. and Saravanamuttoo, H.I.H. Digital Computer Methods for Prediction of Gas Turbine Dynamic Response, SAE Technical Paper 710550, 1971.
[16] Palmer, J.R. and Yan, C. TURBOTRANS—A Programming Language for the Performance Simulation of Arbitrary Gas Turbine Engines with Arbitrary Control Systems, ASME paper, 82-GT-200.
[17] Ramsden, K.W.P. *Aerodynamics Design of Turbomachinery*, *MSc course notes*, Cranfield University, 2013.
[18] Priyant Mark, C. and Selwyn, A. Design and analysis of annular combustion chamber of a low bypass turbofan engine in a jet trainer aircraft, *Propul Power Res*, 2016, **5**, (2), pp 97–107.
[19] Kypyuros, J. and Melcher, K. A reduced models for prediction of thermal and rotational effects on turbine tip clearance, NASA/TM, 2003.
[20] Li, Z. Aircraft engine transient performance modelling with heat soakage effects, PhD Thesis, Cranfield University, 2020.
[21] Kurzke, J. Gas turbine performance commercial software with GasTurbTM, www.gasturb.de, 2016.

Cite this article: Li Z., Li Y.-G. and Sampath S. (2022). Aeroengine transient performance simulation integrated with generic heat soakage and tip clearance model. *The Aeronautical Journal*, **126**, 1265–1287. https://doi.org/10.1017/aer.2022.15